AIAA JOURNAL
Vol. 47, No. 12, December 2009

Cyclic Buckling Tests Under Combined Compression and Shear on Composite Stiffened Panels

P. Cordisco* and C. Bisagni†
Politecnico di Milano, 20156 Milano, Italy

DOI: 10.2514/1.42309

The results obtained on two closed structural boxes composed by four graphite-epoxy curved stringer-stiffened panels, and manufactured by Agusta/Westland, are presented. The closed-box configuration allowed easily applying shear on each panel by subjecting the box to a torsion moment. The boxes were tested under combined axial compression and torque loading, both statically and cyclically. The tests allowed, on one hand, evaluating the effect of different procedures of loading application and, on the other hand, to investigate the influence of cyclic postbuckling combined loads in terms of global and local behaviors, as well as in terms of collapse modalities. The results show the reliability of these structures to safely operate in the postbuckling field, even when the buckling load is reached thousands of times during the operative life.

I. Introduction

DURING the last two decades, the use of composite material in aerospace industries has become more and more widespread. This is basically due to the fact that all of the possibilities offered by the traditional metallic alloy materials seem to be exhausted and a further weight savings in aerospace structures using such materials appears to be difficult. Consequently, the attention of designers focused on this relatively new class of materials in order to realize structures that can be more and more efficient. Among composites, the most promising one is the graphite epoxy, because of its high ratios of strength over weight and of stiffness over weight. With its use being quite recent, at least as far as the primary structures of commercial aviation are concerned, several phenomena still have to be deeply investigated.

One of these phenomena is the postbuckling field [1]. Nowadays, it seems evident that graphite-epoxy stiffened structures can work in the postbuckling range [2–8], but little data deals with the effect that repeated buckling has on the structural response. Indeed, although some results in literature [9–12] are available on the influence that a repeated postbuckling load has on metallic alloy structures, very few studies [13–15] have been published regarding how the cyclic buckling influences the nonlinear response and the collapse modalities of graphite-epoxy panels or how deep into the postbuckling field it is possible to operate without losing structural safety, especially if combined loadings are considered.

The lack of data results in overconservative design criteria: actually, aerospace designers avoid graphite-epoxy structures working in the postbuckling field, placing the limit load below the buckling one [16]. Large weight savings could be achieved if the capability is demonstrated for composite structures to operate in the postbuckling field thousands of times without losing efficiency. In this way, indeed, it will be possible to include the buckling load in the range of the loads allowed during the operative life and to move up the design ultimate load near the collapse. Basically, the challenge is to reach the same level of knowledge for composite structures as for metal alloy structures, for which the phenomena of postbuckling, plasticity, and fatigue are well known [17].

The study presented here is part of the European research project COCOMAT [18] (Improved Material Exploitation at Safe Design of Composite Airframe Structures by Accurate Simulation of Collapse), aiming to exploit the postbuckling field of graphite-epoxy stiffened panels until collapse by means of experimental tests and to develop validated tools able to capture the damage mechanisms.

This paper presents the experimental results achieved at the Politecnico di Milano on two closed structural boxes, obtained by assembling graphite-epoxy stiffened curved panels. The purpose of the tests is to investigate the behavior of the panels under combined axial compression and shear loading. For this reason, because the loading of single curved panels under shear is quite complicated, it was decided to assemble the panels in a closed-box configuration, to apply shear on each panel by testing the box under torque [19]. The design of the boxes [20] was performed at Politecnico di Milano using finite element dynamic explicit analyses carried out in ABAQUS/Explicit.

Two boxes were tested under various combinations of axial compression and torsion. The first box is tested by static loading, and both static and cyclic tests are performed on the second box. Both boxes are then tested until collapse under static combined loading.

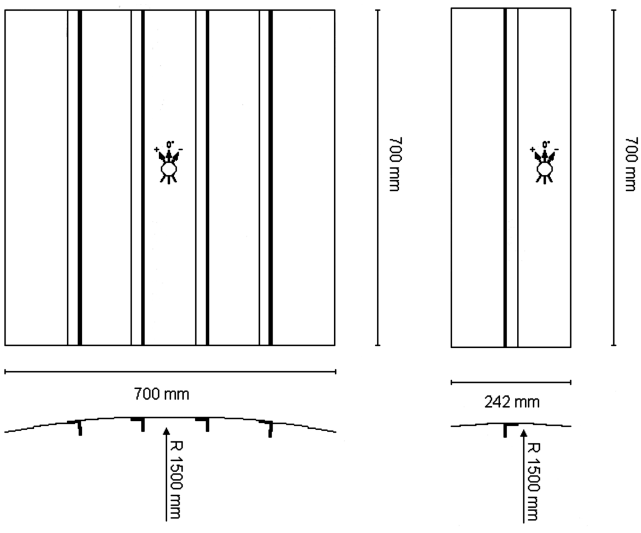

Fig. 1 Panels.

Presented as Paper 2124 at the 49th AIAA/ASME/ASCE/AHS/ASC Structures, Structural Dynamics, and Materials Conference, Schaumburg, IL, 7–10 April 2008; received 21 November 2008; revision received 31 May 2009; accepted for publication 18 August 2009.

*Postdoctoral Fellow, Department of Aerospace Engineering, Via La Masa 34.

†Associate Professor, Department of Aerospace Engineering, Via La Masa 34. Member AIAA.

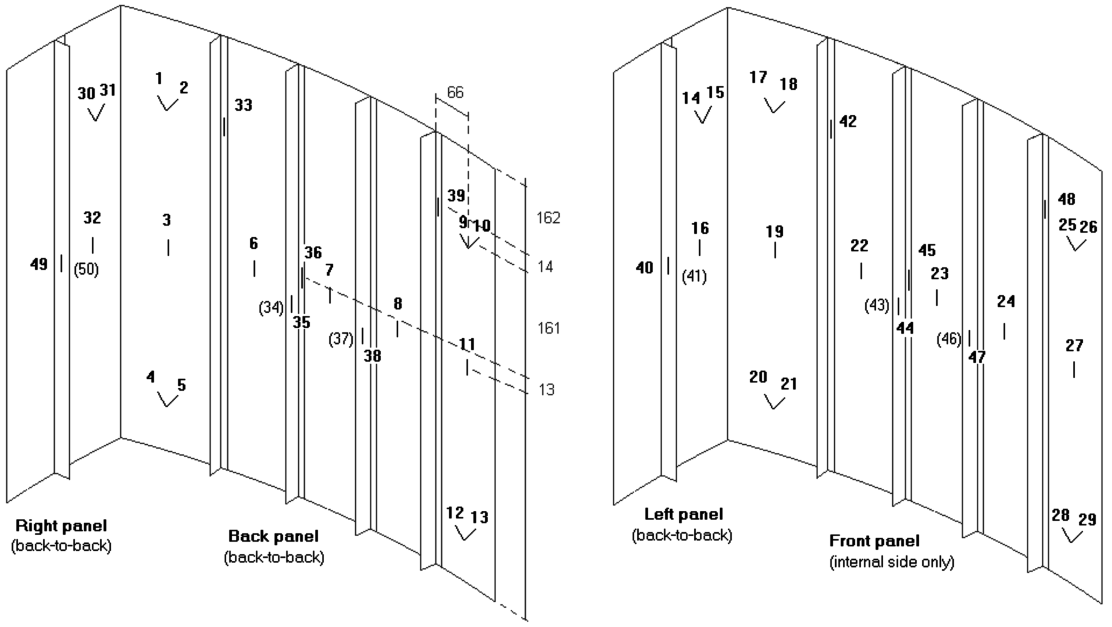

Fig. 2 Strain gauge map.

a) **b)**

Fig. 3 Closed box a) without and b) with aluminum tabs and strain gauges.

Table 1 Materials properties

	Unidirectional	Fabric
Ply thickness, mm	0.15	0.33
Tensile modulus E_{11}, MPa	128052	58447
Tensile modulus E_{22}, MPa	8609	58783
Poisson coefficient ν_{12}	0.302	0.0483
Tensile strength σ_{11}, MPa	1817	443
Tensile strength σ_{22}, MPa	41	420
Shear in plane modulus G, MPa	4666	3065
Shear in plane strength τ, MPa	75	99
Compression modulus E_{11}, MPa	114230	53686
Compression modulus E_{22}, MPa	9342	57765
Compression strength σ_{11}, MPa	1074	466
Compression strength σ_{22}, MPa	103	469
Interlaminar shear strength, MPa	69	78

The aim is to investigate the behavior of these structures in the deep postbuckling field, the effect of different procedure of combined loading application, and the influence of repeated postbuckling combined loads, in terms of global response by means of load-vs-displacement curves and of postbuckling deformation shapes and in terms of local behavior by means of strain gauge measurements and failure modality.

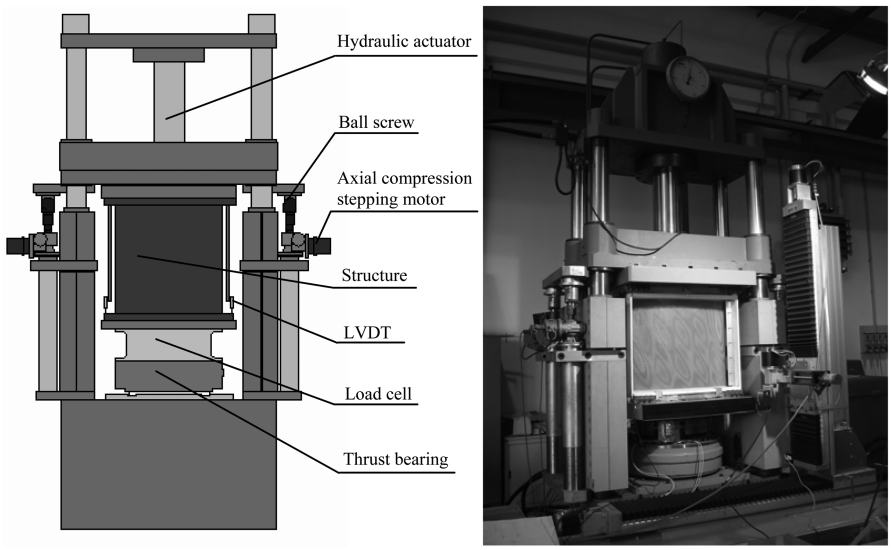

Fig. 4 Sketch and photograph of the buckling test equipment (front view).

Table 2 Thickness and layup (F denotes fabric and UD denotes unidirectional)

Skin thickness	0.99 mm
Skin layup	$[0_F°/-45_F°/0_F°]$
Stringer thickness	2.22 mm
Stringer layup	$[0_F°/0_{UD}°/0_{UD}°/+45_F°/0_{UD}°/0_{UD}°/-45_F°/0_{UD}°/0_{UD}°/0_F°]$

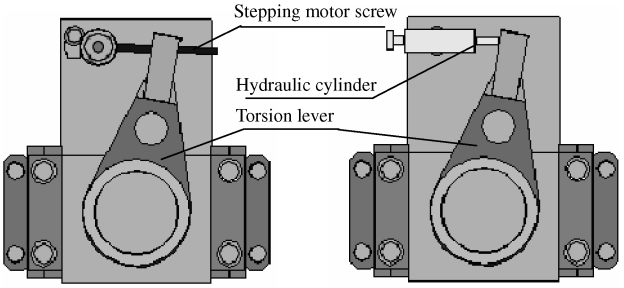

a) b)

Fig. 5 Sketch of the buckling test equipment (top view): a) static modality and b) cyclic modality.

II. Structures

The structural boxes were manufactured by Agusta/Westland. Each box is composed by four panels, for which the dimensions are reported in Fig. 1. Two panels are 700 mm wide and present four stiffeners, and the other two panels are 242 mm wide and present only one stringer in the middle. All of the panels present a radius of curvature of 1500 mm and a height of 700 mm. The stringers are L-shaped with a section of 28 mm × 28 mm and a height of 700 mm and are bonded to the panel skin only after the curing process. Large and small panels were joined together with four more stringers as connection elements, which are identical to the other stringers but present an angle between the flanges equal to 107° instead of 90° and which are applied at the corners of the box using both glue and rivets.

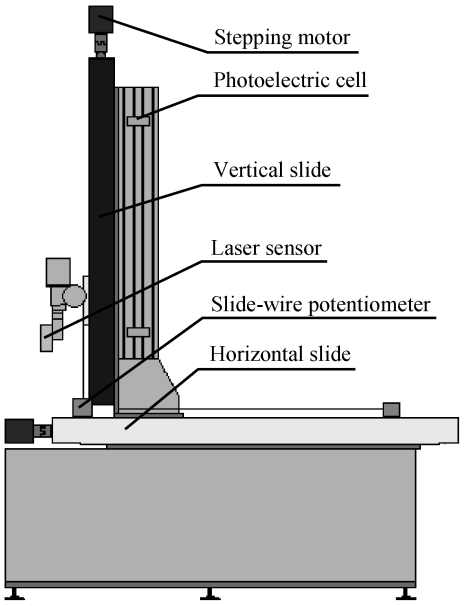

Fig. 6 Sketch of the laser system equipment.

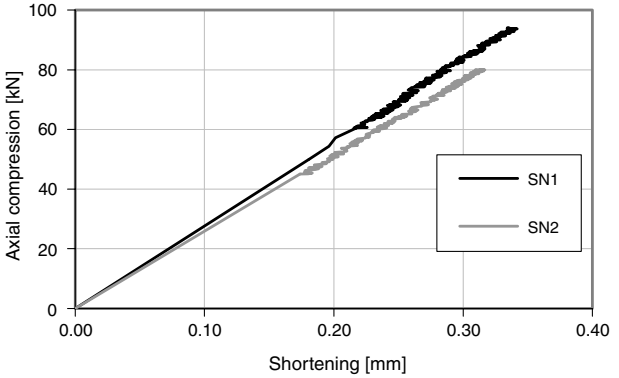

Fig. 7 Axial compression-vs-shortening curves in axial compression tests on box SN1 and box SN2.

Table 3 Experimental tests overview (CW denotes clockwise and CCW denotes counterclockwise)

Test modality	Load conditions
	Box SN1
Static	
Pure compression	Compression
Pure torque	CCW torque
Pure torque	CW torque
Combined tests (8 tests)	Constant compression + CW or CCW torque
Combined tests (8 tests)	Constant CW or CCW torque + compression
Combined tests (8 tests)	Compression + CW or CCW torque increased by steps
Collapse	Constant compression + CCW torque
	Box SN2
Static	
Pure compression	Compression
Pure torque	CCW torque
Combined tests (4 tests)	Constant compression + CCW torque
Collapse	Constant compression + CCW torque
Cyclic	Constant compression + 0 < CCW torque < $125\%T_{BUCKL}$
Cyclic	Constant compression + 0 < CCW torque < $150\%T_{BUCKL}$
Cyclic	Constant compression + 0 < CCW torque < $175\%T_{BUCKL}$

Table 4 Results of axial compression and torsion tests on SN1 and SN2

Test	Measure	SN1	SN2	Difference %
Pure axial compression	Buckling load	75 kN	64 kN	−14.7
Pure axial compression	Initial stiffness	278 kN/mm	254 kN/mm	−8.6
Pure torque	Buckling torque	8.4 kNm	8.1 kNm	−3.6
Pure torque	Initial stiffness	35.9 kNm/ deg	34.9 kNm/ deg	−2.8

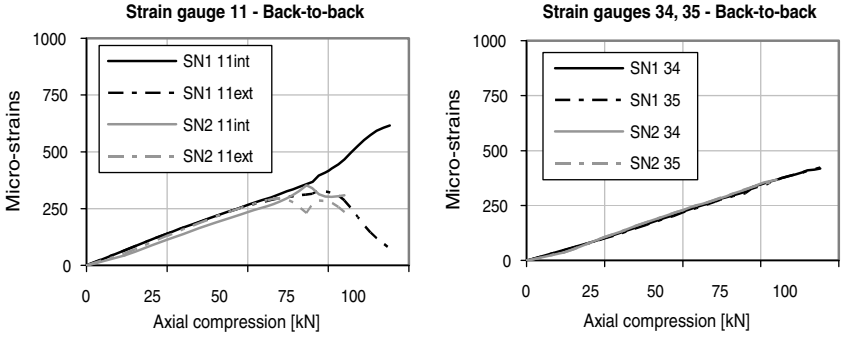

a) Back panel – skin **b) Back panel – stringer**

Fig. 8 Measurements of strain gauges in axial compression tests on box SN1 and box SN2.

The panels are manufactured with unidirectional material and with fabric. The material properties are summarized in Table 1, and the layup and the thickness of skin and stringers are reported in Table 2.

Two aluminum ending tabs are added to the boxes to allow the clamping into the loading machine. A dedicated equipment is used for the bonding process to ensure the correct alignment and the parallelism between the ending tabs, in order to guarantee the uniform distribution of the load during the tests. The free length of the box is consequently reduced to 640 mm.

Each box is then instrumented with 72 strain gauges, for which the position is reported in Fig. 2. In particular, the strain gauges are placed in a back-to-back configuration on one of the large panels (the back panel) and on the two small lateral panels. On the remaining large panel (the front panel), the strain gauges are attached only internally, to leave the external surface free for the out-of-plane displacement measurements.

A photograph of the box as it appears before and after the application of the aluminum tabs and of the strain gauges is presented in Fig. 3.

III. Experimental Equipment

The buckling tests are performed with the equipment reported in Fig. 4. It allows applying both axial compression and torque, applied individually or in combination [4,21]. The axial compression can be applied only statically, whereas it is possible to apply torsion both statically and cyclically.

At the beginning of the test, the axial compression load, imposed using a hydraulic actuator, is supported by four vertical ball screws. Then, during the test, the displacement of the screws is regulated through four PC-controlled stepping motors that guarantee a precision in the applied displacement of ± 0.01 mm. In this way, the

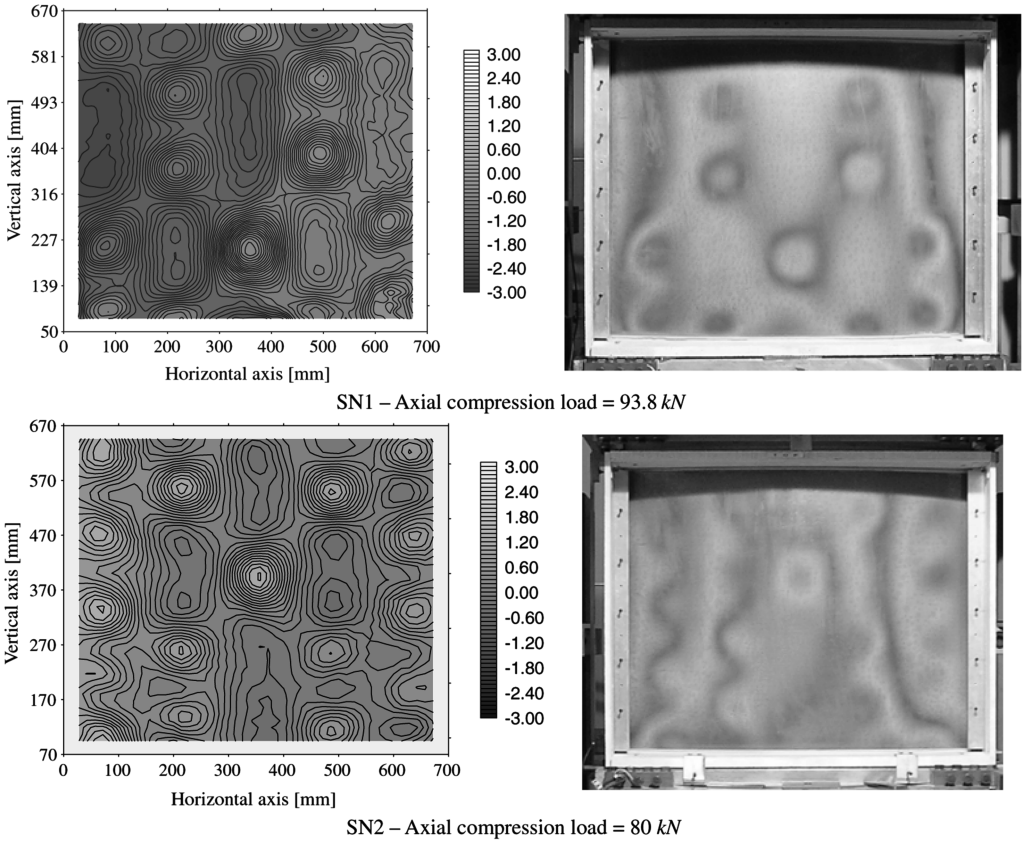

Fig. 9 Laser measurements and photographs with moiré fringes of box SN1 and box SN2 in axial compression tests.

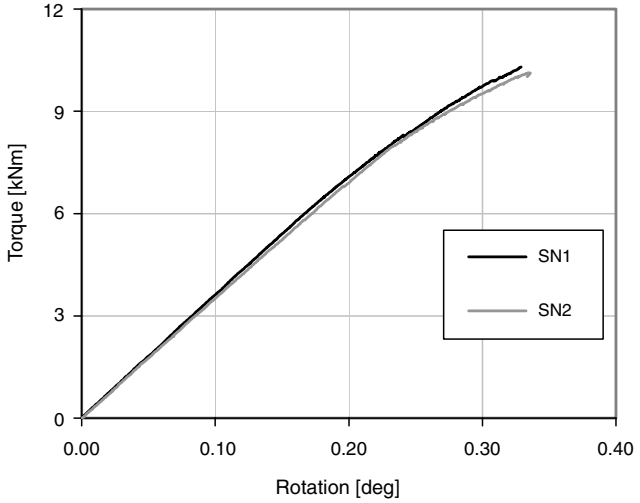

Fig. 10 Torque-vs-rotation curves in the counterclockwise torsion tests on box SN1 and box SN2.

load can be gradually transferred to the test structure in displacement control.

In the static torsion tests, the rotation is imposed using a ball screw connected to a torsion stepping motor (Fig. 5a). The lower part of the structure is able to rotate with an accuracy equal to $\pm 0.0005°$, due to a PC-controlled stepping motor, a lever, and a thrust bearing, whereas the upper part of the structure is fixed.

In the cyclic torsion tests, the stepping motor and the torsion screw are substituted with a hydraulic cylinder driven by a servo valve (Fig. 5b). The torque is transmitted to the structure by controlling the displacement of the cylinder shaft with a linear variable differential transformer (LVDT).

During all of the buckling tests, the load and the torque applied on the testing structure are measured using a three-point load cell, for which the resolution is equal to ± 50 N in compression and ± 5 Nm in torsion, and the shortening and the rotation are recorded by two LVDTs each, for which the accuracy is equal to ± 0.005 mm.

The out-of-plane displacements of the box front panel are measured using a laser system equipment sketched in Fig. 6 that is placed in front of the buckling test equipment, as shown in Fig. 4. It allows measuring the evolution of the deformed shape of the box

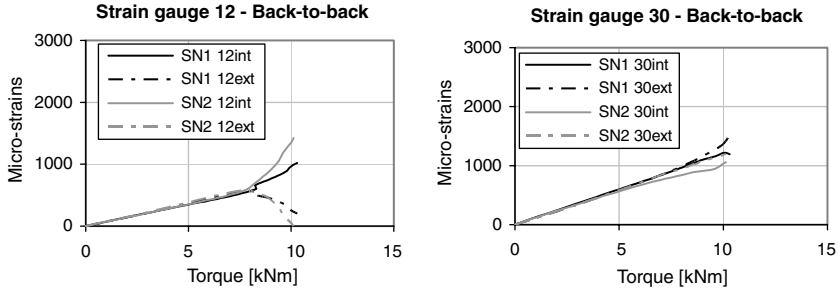

a) Back panel – skin **b) Right panel – skin**

Fig. 11 Measurements of strain gauges in torsion tests on box SN1 and box SN2.

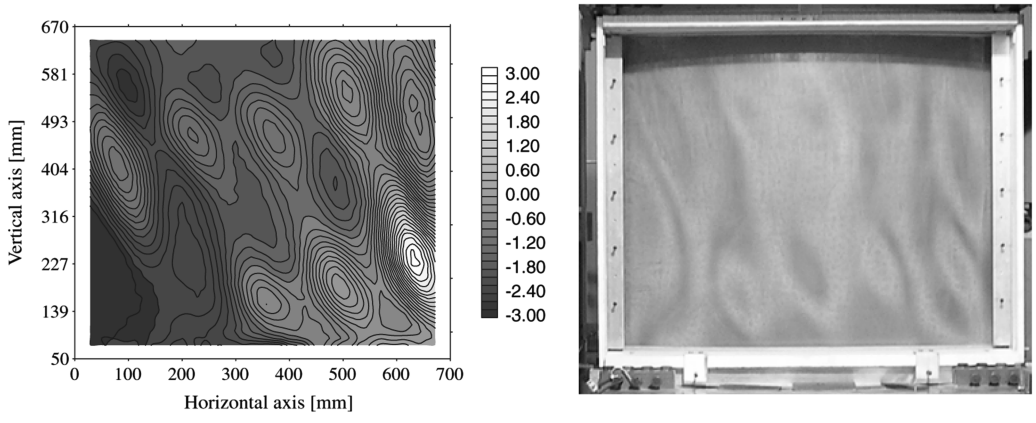

SN1 – Torque = 10.4 *kNm*

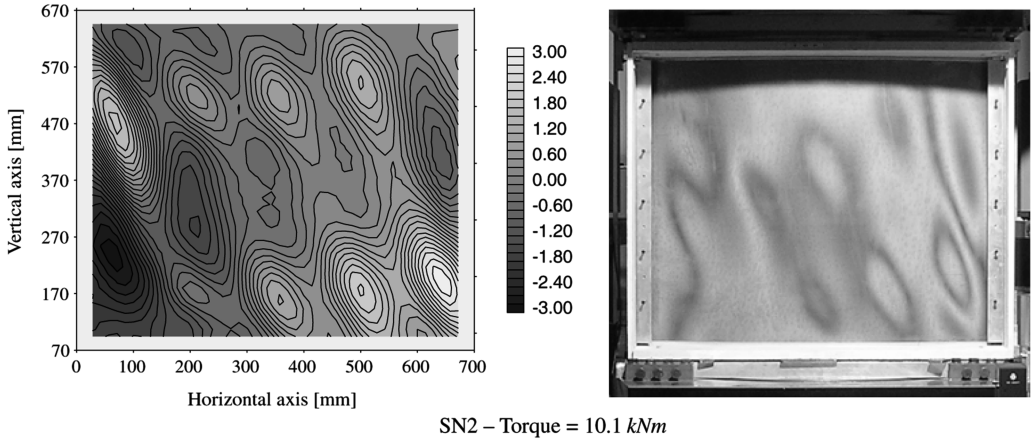

SN2 – Torque = 10.1 *kNm*

Fig. 12 Laser measurements and photographs with moiré fringes of box SN1 and box SN2 in torsion tests.

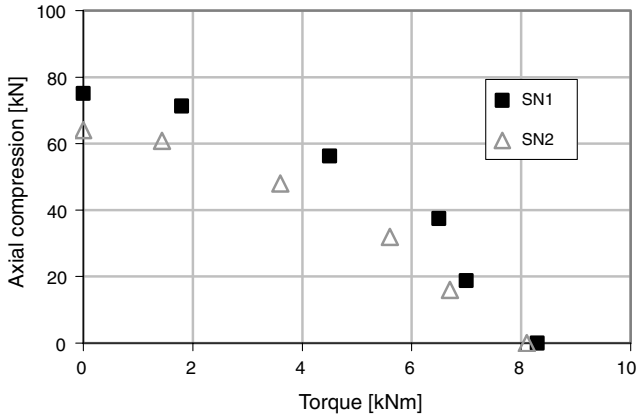

Fig. 13 Comparison of interaction curves of box SN1 and box SN2.

front panel. It consists of a laser sensor (for which the resolution is equal to 50 μm) that is able to translate horizontally and vertically with respect to the box using two stepping motors connected to high-precision slides based on ball screws. The laser position is computer-controlled due to a pair of slide-wire potentiometers, and the start and end of the measurements are given by two pairs of photoelectric cells.

Table 5 Buckling loads and torques in static tests on box SN1 and box SN2

SN1		SN2	
Buckling axial load, kN	Buckling torque, kNm	Buckling axial load, kN	Buckling torque, kNm
64.0	0.0	75.0	0.0
60.8	1.4	71.2	1.8
48.0	3.6	56.2	4.5
32.0	5.6	37.5	6.4
16.0	6.7	18.7	7.0
0.0	8.1	0.0	8.3

Table 6 Buckling loads and buckling torque measured in static tests on box SN1

Test procedure	Buckling axial load, kN	Buckling torque, kNm
Compression	75.0	0.0
CCW torque	0.0	8.3
CW torque	0.0	−7.2
First	71.2	−2.4
First	56.2	−3.6
First	37.5	−5.0
First	18.7	−6.0
First	71.2	1.8
First	56.2	4.5
First	37.5	6.4
First	18.7	7.0
Second	66.0	−2.4
Second	54.0	−3.6
Second	36.0	−5.0
Second	18.0	−6.0
Second	69.8	1.8
Second	52.4	4.5
Second	34.0	6.5
Second	18.0	7.0
Third	67.8	−2.2
Third	56.0	−3.6
Third	37.5	−4.9
Third	19.4	−6.0
Third	65.7	1.6
Third	51.2	4.0
Third	35.6	6.0
Third	18.9	7.0

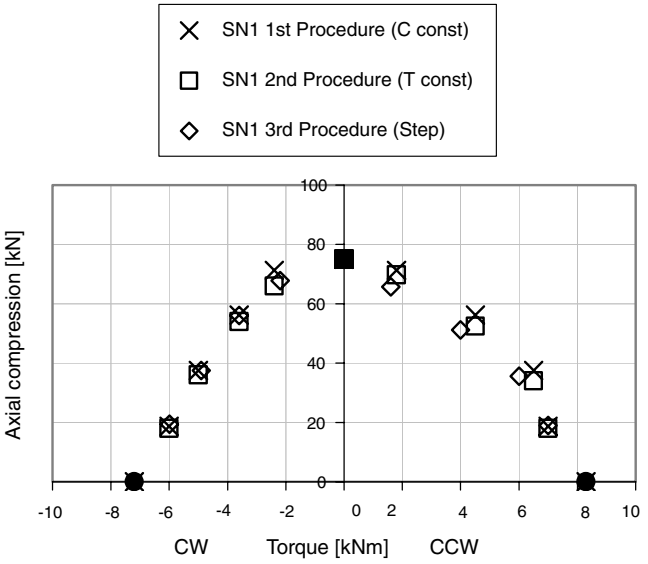

Fig. 14 Interaction curves of box SN1 according three different procedures of loading application.

A moiré fringe system is placed in front of the box in order to visualize the out-of-plane displacements.

IV. Testing Methodology

The testing procedure is decided together with Agusta/Westland and is summarized in Table 3. Two boxes, nominally identical, are tested. The first structure, named SN1, is tested under static loading, and the second structure, named SN2, is tested both statically and under repeated postbuckling loading.

On the first structure, box SN1, 28 static buckling tests are performed. At the beginning, a pure axial compression test, a pure clockwise torque test, and a pure counterclockwise torque test are carried out. Then eight interaction points with combined compression and torsion are performed using three different procedures. In the first procedure, the axial compression is fixed to constant values (equal to 25, 50, 75, and 95% of the buckling load recorded in the pure axial compression test), and the postbuckling field is reached by increasing the torque, both in the clockwise direction and in the counterclockwise direction. In the second procedure, the torque is fixed to constant values (equal to the buckling torque recorded in the tests performed with the first procedure), and the postbuckling field is

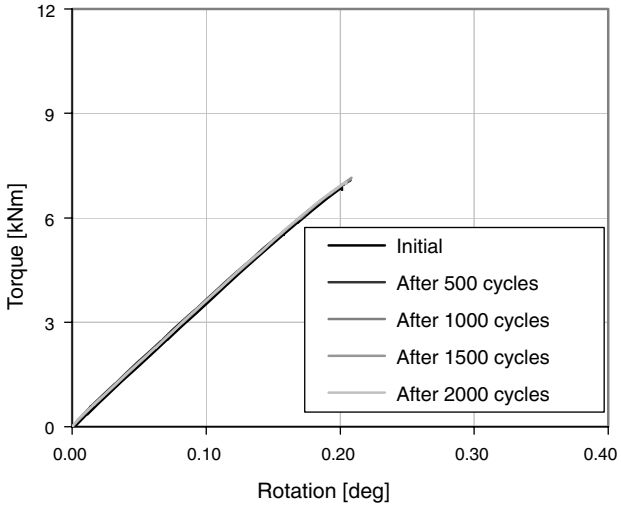

Fig. 15 Comparison of torque-vs-rotation curves measured during cyclic sequence at 125% T_{BUCKL}.

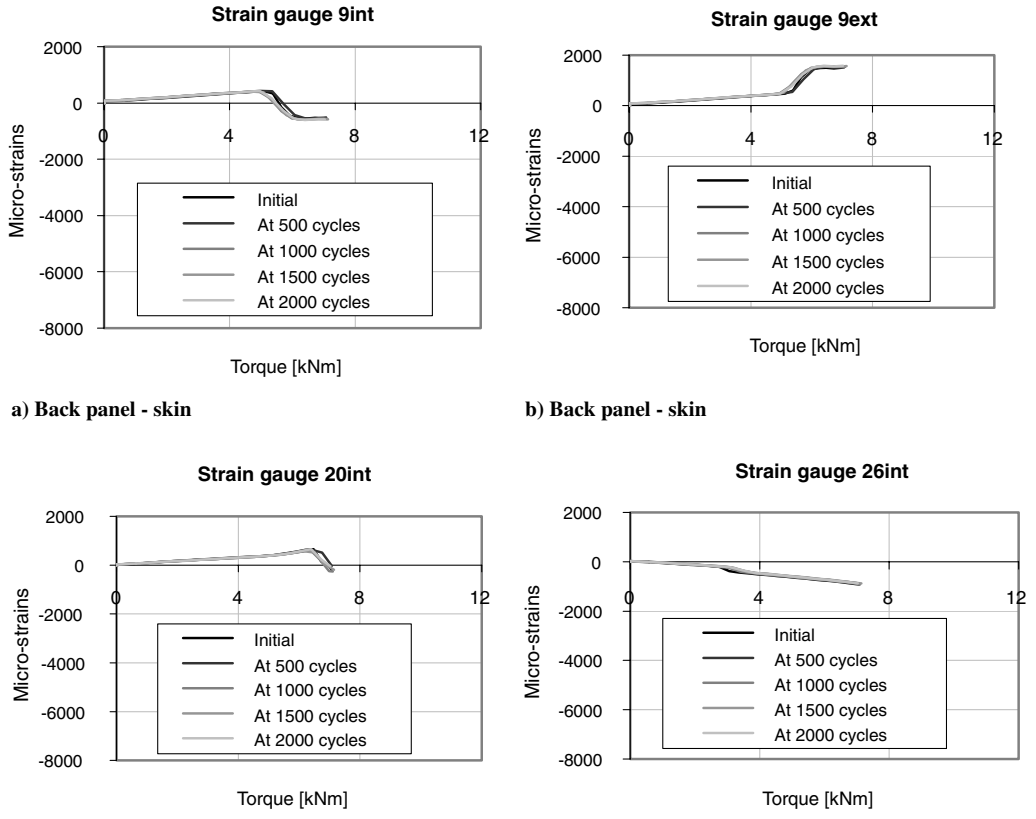

a) Back panel - skin

b) Back panel - skin

c) Front panel - skin

d) Front panel - skin

Fig. 16 Comparison of strain gauge curves measured in cyclic sequence at 125% T_{BUCKL}.

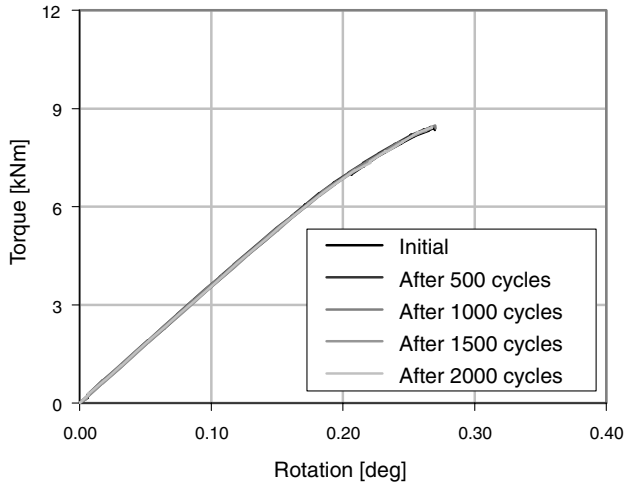

Fig. 17 Comparison of torque-vs-rotation curves measured during cyclic sequence at 150% T_{BUCKL}.

reached by increasing the axial compression. Finally, in the third procedure, the axial compression and the torque are increased by steps equal to 5% of the buckling loads measured in the tests carried out with the first procedure. In all of the combined tests, the maximum reached value is 125% of the buckling load. Box SN1 is then tested until collapse, keeping the axial compression equal to 50% of the buckling load measured in the pure axial compression test and reaching the collapse by increasing the torque in the counterclockwise direction.

On the second structure, box SN2, six static tests are performed in order to measure the interaction curve: a pure axial compression test, a pure counterclockwise torque test, and four combined tests in the counterclockwise direction according to the first procedure, with fixed axial compression and increasing torque. Box SN2 is then tested under cyclic loading in three cyclic sequences performed at 0.2 Hz, fixing the axial load to 50% of the buckling load recorded in the pure axial compression test and cycling the torque in the following way: 1) 2000 cycles from 0 to 125% of the buckling torque, 2) 2000 cycles from 0 to 150% of the buckling torque, and 3) 2000 cycles from 0 to 175% of the buckling torque.

The choice of 2000 cycles is related to the estimation of the number of times that this type of structure enters the postbuckling range during its operative life, given by Agusta/Westland.

Every 500 cycles, the torque-vs-rotation curve, the strain gauge measurements, and the laser scan of the box front panel are taken. Box SN2 is then statically tested until collapse, performing the collapse test in the same conditions as with the collapse test of box SN1.

V. Experimental Results

The results of the experimental tests are presented in four different sessions, in order to highlight the following aspects: 1) buckling behavior under static loading and differences between nominally identical boxes, 2) effect of loading sequence on buckling behavior under combined axial compression and torque, 3) effect of cyclic postbuckling combined loading, and 4) collapse modalities after static and cyclic tests.

A. Buckling Behavior Under Static Loading and Differences Between Nominally Identical Boxes

The two boxes are initially statically tested under pure axial compression and under pure torque until 125% of the buckling loads in order to record the static behaviors.

The buckling loads are measured using the strain gauges in a back-to-back configuration, taking into account the fact that the prediction of the first buckling load is difficult to determine due to the difficulty with unambiguously defining the buckling onset and due to the

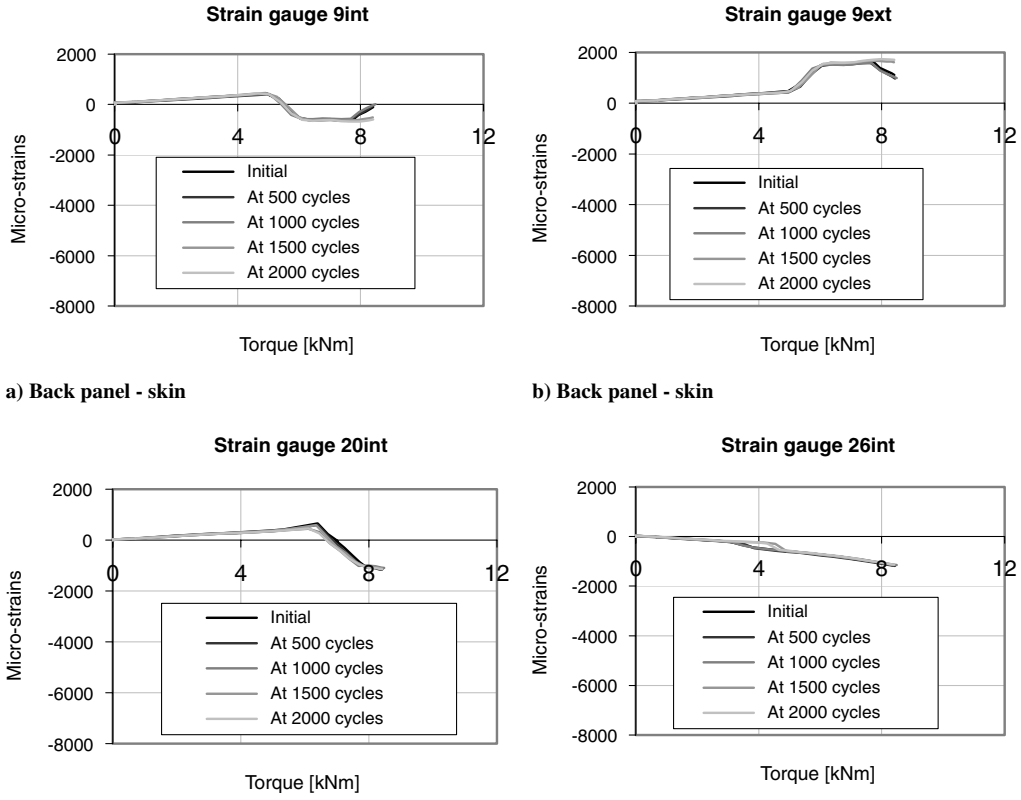

a) Back panel - skin **b) Back panel - skin**

c) Front panel - skin **d) Front panel - skin**

Fig. 18 Comparison of strain gauge curves measured in cyclic sequence at 150% T_{BUCKL}.

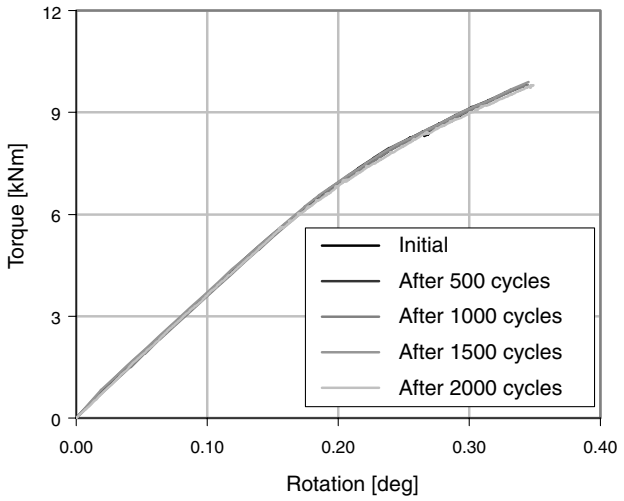

Fig. 19 Comparison of torque-vs-rotation curves measured during cyclic sequence at 175% T_{BUCKL}.

number of strain gauges. The buckling loads obtained in the pure axial compression and in the pure torque tests on the two boxes are reported in Table 4, in which they are compared taking box SN1 as reference.

Even if the two boxes are nominally identical, some differences are measured, especially as far as the buckling load of pure axial compression tests is concerned. The buckling load of box SN2 is 14.7% lower than the buckling load of box SN1.

Comparing the stiffness of the boxes, the difference is lower, as shown in Fig. 7, in which the axial compression-vs-shortening curves measured during the pure axial compression tests on box SN1 and box SN2 are superimposed. The initial axial stiffness of box SN2, calculated as the slope of the curve up to 85% of the buckling load, is 8.3% lower than that of box SN1. The stiffness of the curves does not change after the buckling load, as the largest part of the axial load is withstood by the stringers after the skin buckles.

The initial strain distribution is the same for the two boxes, but then the strain gauges bonded on the skin of box SN2 show a lower buckling load (Fig. 8a). On the contrary, no difference in strain distribution is observed for the stiffeners (Fig. 8b).

The laser measurements and the photographs with moiré fringes of the postbuckling deformation of the two boxes at 125% of the buckling compression loads are reported in Fig. 9.

The load values at which the laser scan are taken are different, because the 125% of the buckling loads are equal to 93.8 kN for box SN1 and 80 kN for box SN2. The out-of-plane displacements on box SN1 reach 2.6 mm inward and 0.4 mm outward, and those on box SN2 are 0.6 mm inward and 1.2 mm outward. The buckle distribution is also slightly different.

The differences between the two boxes measured in the pure counterclockwise torque tests are practically negligible, as shown in Table 4. Comparing the torque-vs-rotation curves (Fig. 10), it can be noted that the difference between the initial stiffness, calculated as the slope of the curves up to 85% of the buckling torque, is around 3%. The curves present a knee starting from the buckling torque, after which the slopes are reduced. Indeed, after the skin buckling, the structure, even if is still capable to react the loading increments, offers a lower stiffness, due to the lower contribution of the stringers in withstanding the torque.

The strain distributions are practically the same along the panels of the two boxes, as shown in Fig. 11.

The deformed shapes and the buckles distribution measured on the two boxes at 125% of the buckling torque are also very similar, as shown in Fig. 12. In this case, 125% of the buckling torque corresponds to a very similar torque value (i.e., 10.4 kNm for box SN1 and 10.1 kNm for box SN2). The maximum out-of-plane displacement is equal to 6 mm on both structures, but on box SN1, the

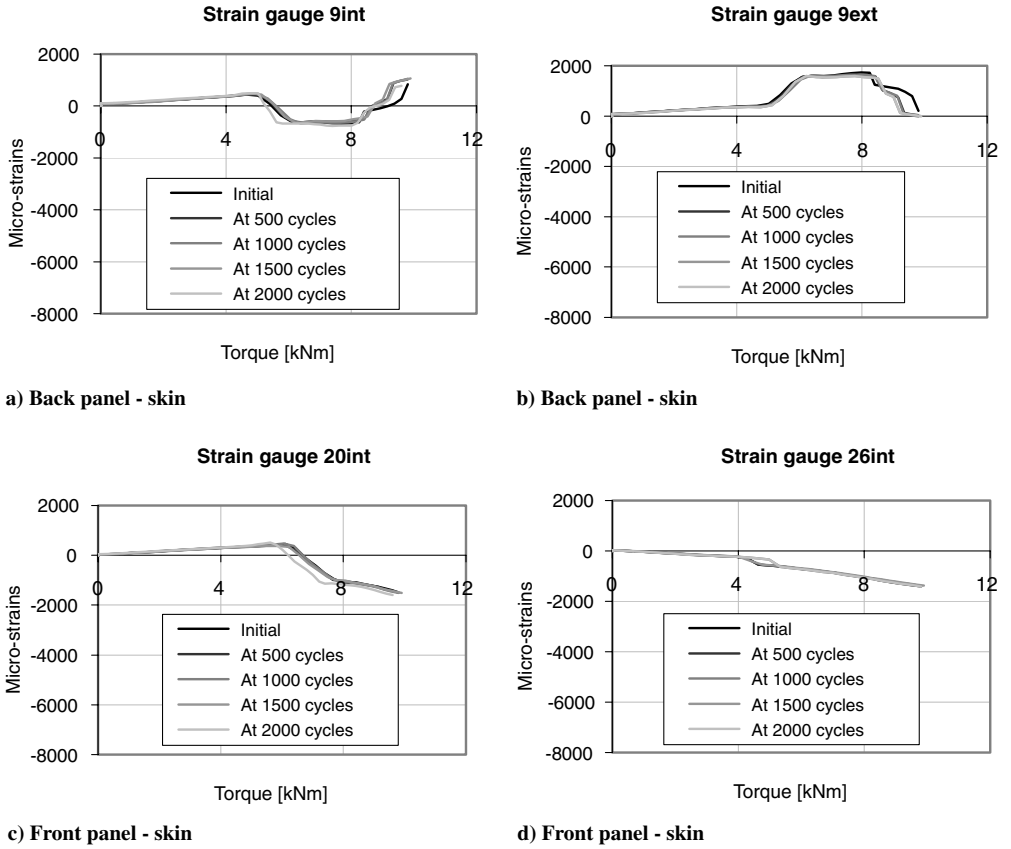

a) Back panel - skin **b) Back panel - skin**

c) Front panel - skin **d) Front panel - skin**

Fig. 20 Comparison of strain gauge curves measured in cyclic sequence at 175% T_{BUCKL}.

buckles are slightly inward-shifted. Indeed, the out-of-plane displacements are 3.5 mm inward and 2.5 mm outward on box SN1 and 3 mm both inward and outward on box SN2.

Four static combined axial compression and torque tests are then carried out on each box, keeping a fixed axial compression (equal to 25, 50, 75, and 95% of the buckling load recorded in the pure axial compression tests) and increasing the torque in the counterclockwise direction up to the 125% of the buckling torque. Table 5 reports the measured buckling loads, and the interaction curves are shown in Fig. 13. The differences between the combined buckling loads measured on the two boxes reach the maximum value in the pure axial compression test and decreases as the contribution of the torque increases.

The main reason for the different behaviors achieved in the static tests is probably due to the manufacturing process. Indeed, many works in literature show that the role played by imperfections is more important under axial compression than under torque [22–25], as slightly different geometries between two nominally identical specimens can modify the buckling load under axial compression, but cannot sensibly change the buckling torque, especially in the case of stiffened structures.

B. Effect of Loading Sequence Under Combined Axial Compression and Torque

To evaluate the effect of the different procedures of loading applications, box SN1 is tested under static combined axial compression and torque, according to three different procedures. In the first procedure, the axial compression is fixed to constant values and the postbuckling field is reached by increasing the torque, both in the clockwise direction and in the counterclockwise direction. In the second procedure, the torque is fixed to constant values and the postbuckling field is reached by increasing the axial compression. In the third procedure, the axial compression and the torque are increased by steps. In all of the combined tests, the maximum reached value is equal to 125% of the buckling load.

In total, 27 static tests are performed on box SN1: a pure axial compression test, two pure torque tests (one in the clockwise and one in the counterclockwise direction), and 24 combined axial compression and torque tests. The measured buckling loads are reported in Table 6, in which positive torque corresponds to the counterclockwise direction. The buckling torques achieved in the pure clockwise and in the pure counterclockwise torque tests are different, due to the unsymmetric L-shaped section of the stringers.

Figure 14 presents the interaction curves measured using the three different loading procedures. Observing the interaction curves, it is evident that the buckling load just depends on the amount of axial compression and torque applied and is independent of the order of application of the loading. It means, for example, that applying an axial compression followed by a torque causes the box to buckle at the same load at which it would buckle by applying a torque followed by an axial compression.

C. Effect of Cyclic Postbuckling Combined Loading

Box SN2 is then tested under cyclic combined axial compression and torque loads. Three sequences are performed, each one of 2000 cycles. The first 2000 cycles are carried out fixing the axial load to 32 kN, equal to 50% of the buckling load measured in the pure axial compression test, and cycling the torque from 0 to 7 kNm, equal to 125% of the buckling torque measured in the corresponding combined static test (test 4 of Table 5). Every 500 cycles, the behavior of the box is investigated by recording the torque-vs-rotation curve and the strain gauge measurements and by scanning the deformed shape with the laser system.

Figure 15 presents the comparison of the five torque-vs-rotation curves. Note that there is no change in the global behavior of the box due to the repetition of the load. The same observation can be done by comparing the strain gauge curves during the application of the cycles (Fig. 16).

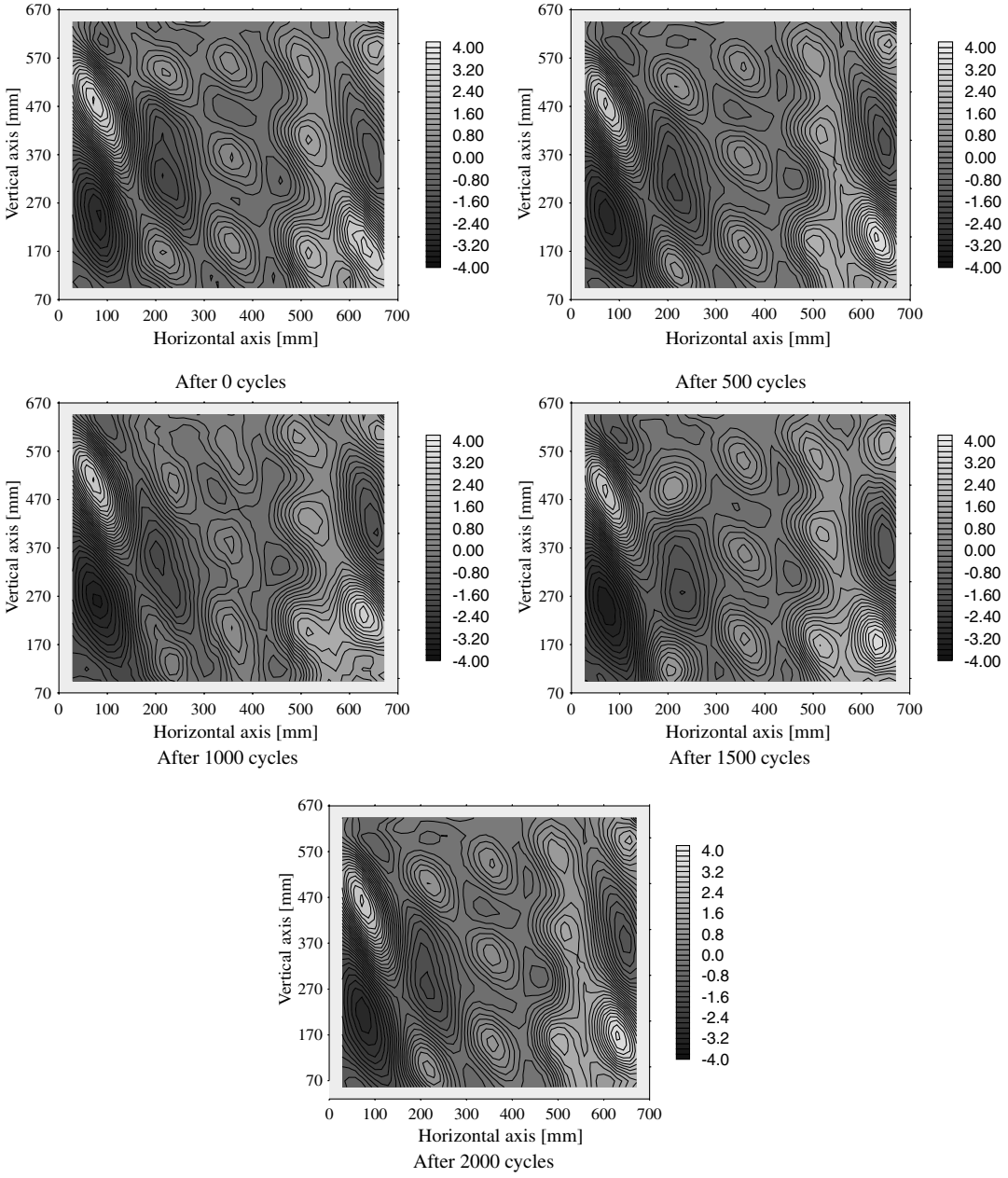

Fig. 21 Comparison of laser measurements during cyclic sequence at 175% T_{BUCKL}.

Box SN2 is then subjected to 2000 more cycles, always fixing the axial load to 32 kN and cycling the torque from 0 to 8.4 kNm, equal to 150% of the buckling torque. Even for this sequence, every 500 cycles, the behavior of the box is investigated by recording the torque-vs-rotation curve and the strain gauge measurements and by scanning the deformed shape with the laser system.

No changes due to the repetition of the postbuckling load are observed, either in the global behavior comparing the torque-vs-rotation curves reported in Fig. 17 or in the local behavior comparing some strain gauge measurements, as shown in Fig. 18.

The last 2000 cycles are performed fixing the axial load to 32 kN and cycling the torque from 0 to 9.8 kNm, equal to 175% of the buckling torque. Even for this load level, the behavior of the box is investigated every 500 cycles. Figure 19 presents the comparison of the five torque-vs-rotation curves. Again, no change is observed in the global behavior of the box, due to the load repetition. The same observation can be done by comparing the strain gauge measurements (Fig. 20) or the external surface of the box front panel as

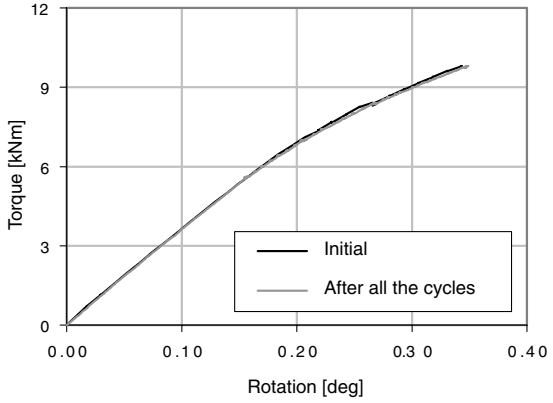

Fig. 22 Comparison of torque-vs-rotation curves measured before and after the cyclic sequences.

Table 7 Results of collapse tests on box SN1 and box SN2

Measure	SN1	SN2	Difference %
Constant axial compression	37.6 kN	32 kN	−14.9
Buckling torque	6.4 kNm	5.6 kNm	−12.5
Collapse torque	20.1 kNm	21.4 kNm	6.5
Initial stiffness	37.0 kNm/ deg	35.6 kNm/ deg	−3.8
Postbuckling stiffness	11.9 kNm/ deg	12.5 kNm/ deg	5
Collapse load and buckling load	3.14	3.82	21.6

scanned by the laser system at the maximum reached torque at 0, 500, 1000, 1500 and 2000 cycles (Fig. 21).

The results obtained on box SN2 show that the cycling loading in the postbuckling field under combined axial compression and torque up to 175% of the buckling torque have no influence on the behavior of these structures. Indeed, if the initial structural response is compared with that obtained at the end of the three cyclic sequences, as shown in Fig. 22, it is possible to observe that the matching between the two curves is perfect. Consequently, this type of structures can safely work even when the postbuckling range up to 175% of the buckling load is reached thousands of times during the operative life. Besides, the displayed behavior seems to allow the conclusion that a cyclic postbuckling design is not needed in these conditions and that these panels can be designed by taking into account only static requirements.

D. Collapse Modalities After Static and Cyclic Tests

The two boxes are finally tested until collapse, keeping the axial compression equal to 50% of the buckling load measured in the pure axial compression test and reaching the collapse by increasing the torque in the counterclockwise direction.

Table 7 summarizes and compares the results obtained in the collapse tests on the two boxes, taken as reference box SN1, and the comparison of the torque-vs-rotation curves obtained in the collapse tests is reported in Fig. 23.

Both boxes present a ratio between collapse load and buckling load greater than three. The largest difference between the structures is found in the buckling loads: the buckling load of box SN2 is 12.5% lower then the buckling load of box SN1. The initial stiffness (calculated as the slope of the curve up to 85% of the buckling load) as well as the postbuckling stiffness (calculated as the slope of the curve from 150% of the buckling torque up to the maximum reached torque) differ only by 4–5%. This is easy to understand, as the collapse tests are performed with a predominant torsion and the static behaviors of the boxes under torque are very similar.

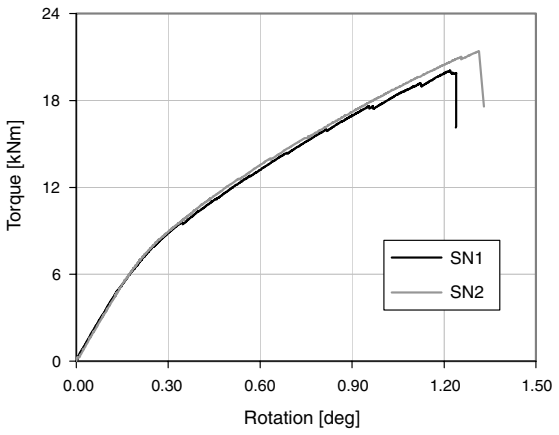

Fig. 23 Torque-vs-rotation curves measured during collapse tests on box SN1 and box SN2.

The evolution of the deformed shape of the two boxes, presented in Figs. 24 and 25, is also very similar. In both cases, the buckling is characterized by few small diagonal waves (Figs. 24a and 25a). As the torque is increased, more waves appear until, at about 13 kNm, two rows of waves are regularly distributed all over the panels (Figs. 24b and 25b). At this load, the out-of-plane displacements are 7 mm deep inward and 5 mm deep outward for box SN1 and 7 mm deep inward and 6 mm deep outward for box SN2.

Further increasing the torque does not change the shape any more, but increases the out-of-plane displacements (Fig. 24c and 25c). The last laser scans are recorded at 19.2 kNm for box SN1 and 21 kNm for box SN2 because of the different collapse loads (Figs. 24d and 25d). The measured out-of-plane displacements are equal to about 10 mm both inward and outward for both boxes.

The two boxes present also similar local behavior, as shown in Fig. 26, in which some strain gauge measurements obtained during the two collapse tests are reported. Some differences can be noted after the skin buckling. The failure mechanisms of the two boxes are the same. Both boxes noisily collapse because of the failure of one of the lateral panels. A large rip is visible on the left small panel starting from the skin, just in correspondence of the area bonded to the corner connection stringer. The rip is generated in the upper left corner on box SN1 and in the lower right corner on box SN2, as shown in Fig. 27. These two areas correspond to the fibers subjected to the maximum stress because of the tension generated by the torsion.

Box SN2, even if cyclically tested under combined postbuckling loads, shows a collapse load equal to 21.4 kNm, which is 6.5% higher then the collapse load of box SN1, equal to 20.1 kNm, which is tested only statically. Considering the differences initially recorded in the static behaviors of the boxes and the fact that the performances of these structures cannot be improved by the cyclic combined loading, it seems reasonable to impute this small difference in the collapse loads to the manufacturing differences between the boxes.

It is thus obtained that the postbuckling combined loading up to 175% of the buckling load, reached thousands of times, does not influence the collapse modalities and the collapse loads. Indeed, the global structural response, the local strain distribution, the evolution of the deformed shapes, and the collapse area of the two boxes are substantially the same.

VI. Conclusions

The behavior of two closed boxes, composed by four graphite-epoxy panels, manufactured by Agusta/Westland, has been experimentally investigated under combined axial compression and torque, both statically and cyclically.

On the first box, 28 static buckling tests were performed applying three different procedures of loading application to obtain the interaction curves. The second box, after six static tests, was subjected to three cyclic sequences, imposing a constant axial compression and cycling the torque from zero to the postbuckling field. Both structures were then collapsed under combined loading in the same conditions.

The results have been presented and compared in terms of buckling load, buckling stiffness, torque-vs-rotation curve, deformed shape, and strain gauge measurements and allow obtaining three main conclusions.

First, by comparing the interaction curves measured on the first box with three different procedures of loading application, it is possible to conclude that the buckling load just depends on the amount of axial compression and torque applied and is independent of the order of application of the load.

Second, by comparing the response of the second box before and after the application of the cyclic postbuckling combined loading, it is possible to observe that the loading repetition does not influence the structural behavior, either in terms of stiffness and buckling load or in terms of deformed shapes and strain levels.

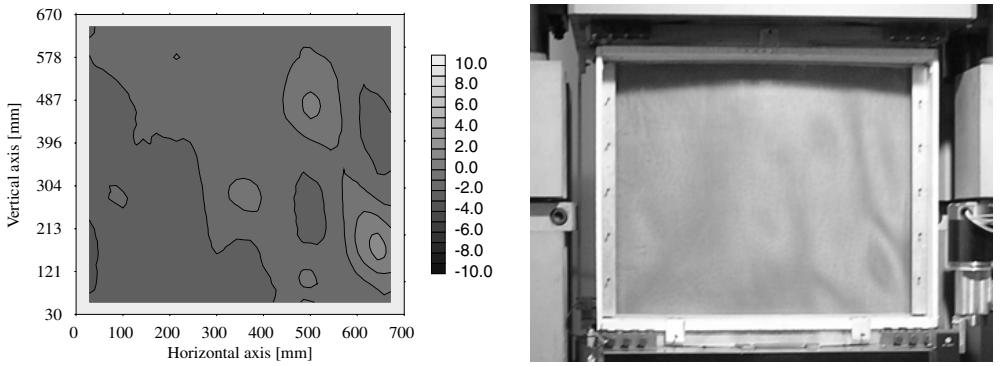

Torque = 6.4 *kNm*; Axial compression = 37.5 *kN*

a)

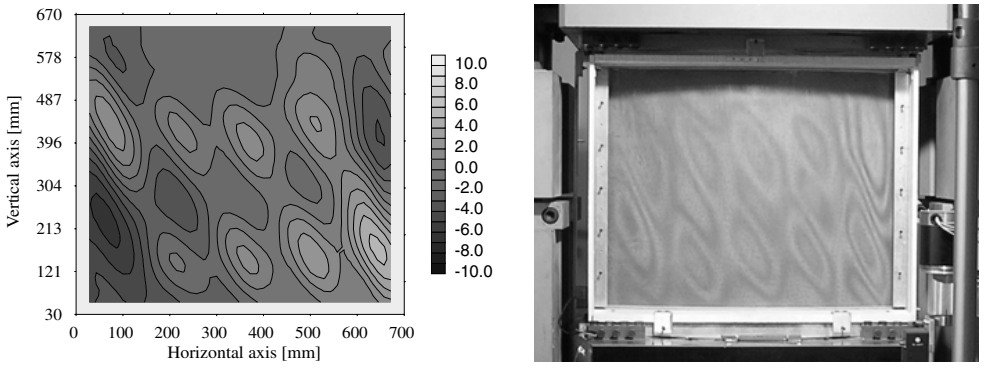

Torque = 12.8 *kNm*; Axial compression = 37.5 *kN*

b)

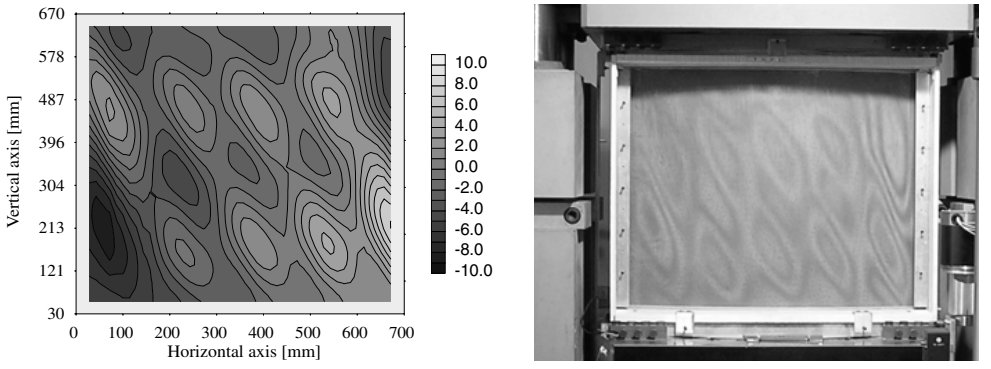

Torque = 16 *kNm* ; Axial compression = 37.5 *kN*

c)

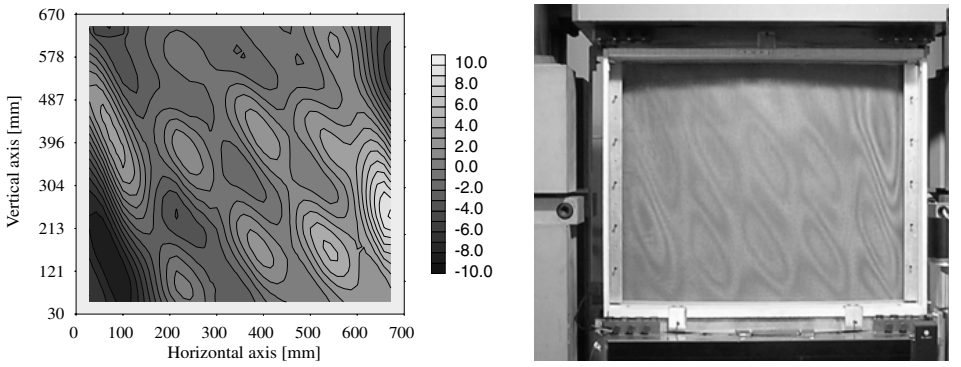

Torque = 19 .2 kNm; Axial compression = 37.5 kN

d)

Fig. 24 Laser measurements and photographs with moiré fringes of box SN1 during collapse test.

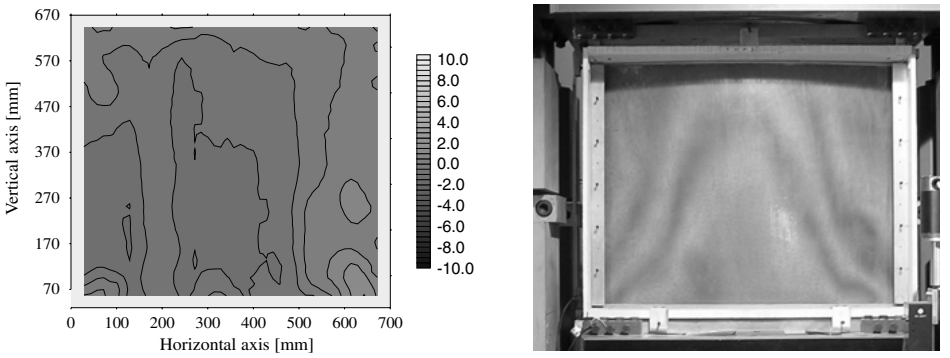

Torque = 5.6 *kNm*; Axial compression = 32 *kN*

a)

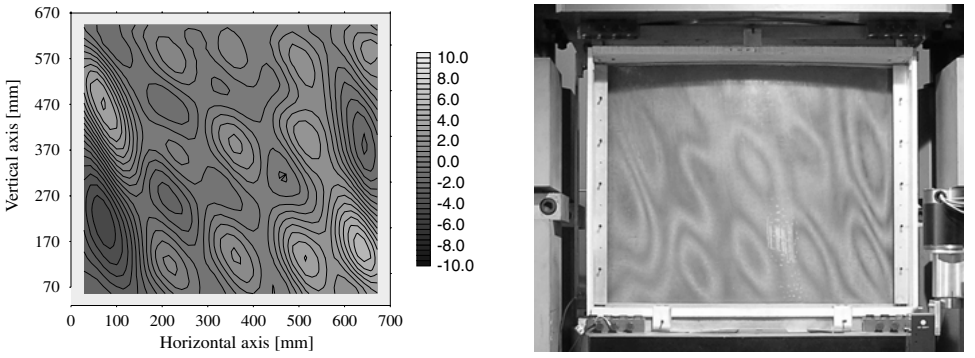

Torque = 12.8 *kNm*; Axial compression = 32 *kN*

b)

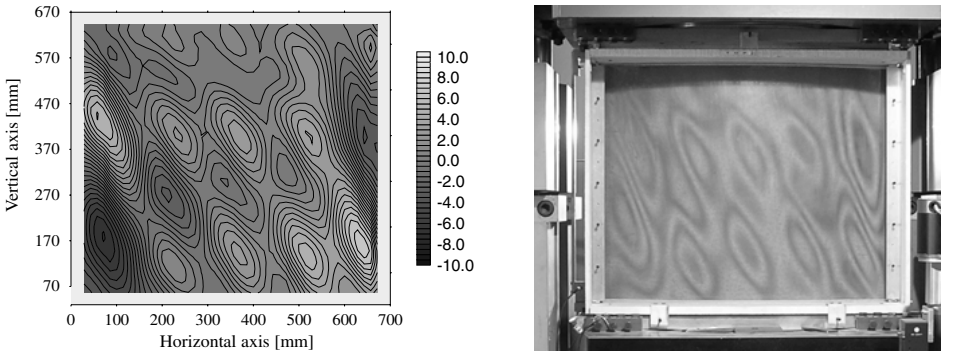

Torque = 16.8 *kNm*; Axial compression = 32 *kN*

c)

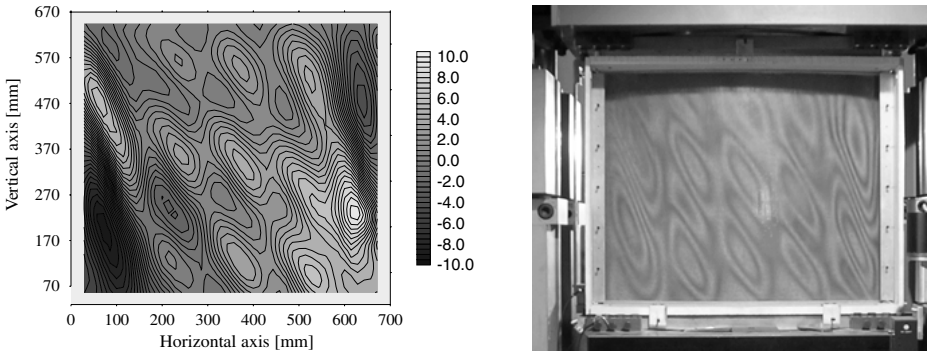

Torque = 21 *kNm*; Axial compression = 32 *kN*

d)

Fig. 25 Laser measurements and photographs with moiré fringes of box SN2 during collapse test.

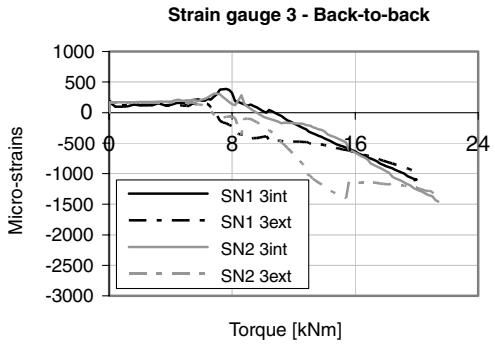

a) Back panel – skin

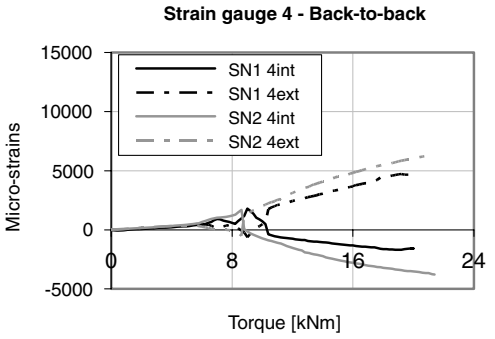

b) Back panel – skin

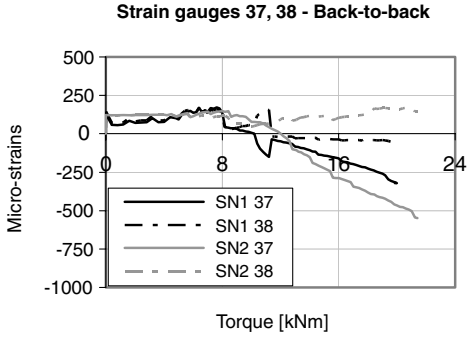

c) Back panel – stiffener

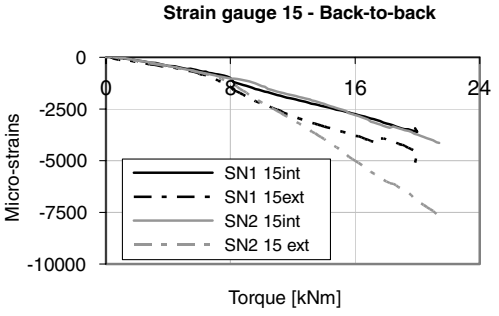

d) Left panel – skin

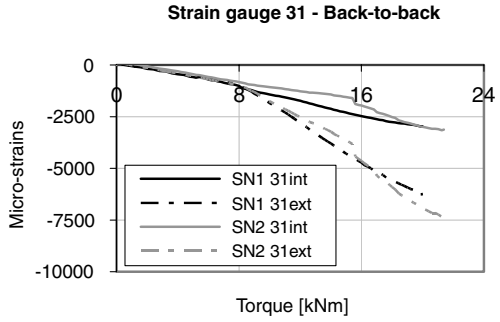

e) Right panel – skin

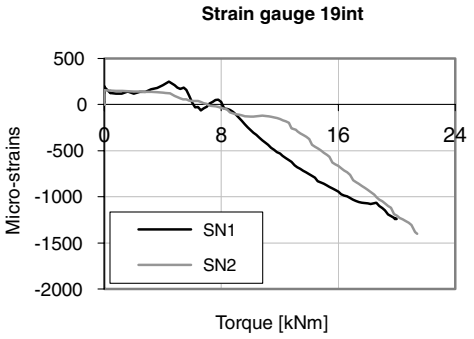

f) Front panel – skin

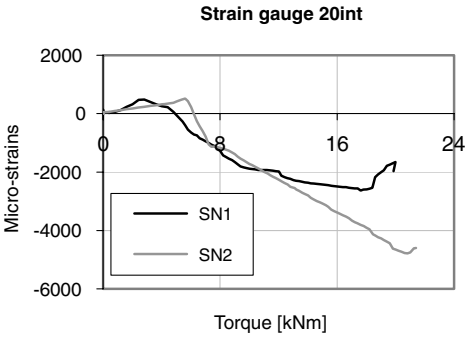

g) Front panel – skin

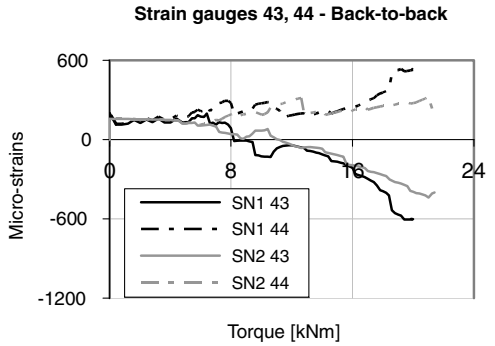

h) Front panel – stiffener

Fig. 26 Measurements of strain gauges in collapse tests on box SN1 and box SN2.

Third, by comparing the responses measured during the collapse tests on the two boxes, it is evident that the cyclic combined loading in the postbuckling field up to 175% of the buckling load, reached thousands of times, has no effect on the global behavior and on the collapse modalities. Indeed, the boxes present the same response in terms of initial and postbuckling stiffness, in terms of strain distribution, and in terms of evolution of deformed shapes. The collapse was due to rips on a lateral panel for both structures.

Consequently, the graphite-epoxy panels investigated here show a large capability to safely work in the postbuckling field, offering ratios between collapse load and buckling load greater than three. Besides, they do not suffer any loss of structural performances, even

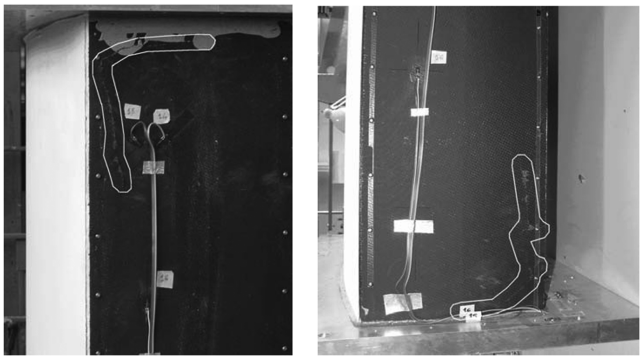

Box SN1 – Left panel Box SN2 – Left panel

Fig. 27 Failure areas on box SN1 and box SN2.

if the postbuckling field is reached thousands of times during the operative life.

Acknowledgments

This work is supported by the European Commission, Competitive and Sustainable Growth Programme, contract no. AST3-CT-2003-502723, project COCOMAT (Improved Material Exploitation at Safe Design of Composite Airframe Structures by Accurate Simulation of Collapse). The authors would like to express their gratitude to Vittorio Giavotto for sharing his expertise and knowledge. The information in this paper is provided as is, and no guarantee or warranty is given that the information is fit for any particular purpose. The user thereof uses the information at its sole risk and liability.

References

[1] Singer, J., Arbocz, J., and Weller, T., *Buckling Experiments—Experimental Methods in Buckling of Thin-Walled Structures*, Vol. 1 and 2, Wiley, New York, 2002.

[2] Knight, N. F., Jr., and Starnes, J. H., Jr., "Postbuckling Behavior of Selected Curved Stiffened Graphite-Epoxy Panels Loaded in Axial Compression," *AIAA Journal*, Vol. 26, No. 3, 1988, pp. 344–352. doi:10.2514/3.9895

[3] Zimmermann, R., and Rolfes, R., "CFRP Fuselage Structures—Postbuckling Permitted," *Air and Space Europe*, Vol. 3, No. 3–4, 2001, pp. 129–131. doi:10.1016/S1290-0958(01)90075-9

[4] Bisagni, C., and Cordisco, P., "Testing of Stiffened Composite Cylindrical Shells in the Postbuckling Range until Failure," *AIAA Journal*, Vol. 42, No. 9, 2004, pp. 1806–1817. doi:10.2514/1.6088

[5] Bisagni, C., and Giavotto, V., "Experiments and Analyses on PostBuckling Behavior of Stringer-Stiffened Laminated Composite Helicopter Tailplanes," 46th AIAA/ASME/ASCE/AHS Structures, Structural Dynamics, and Materials Conference, Austin, TX, AIAA Paper 2005-1866, 2005.

[6] Majeed, M., and Hyer, M. W., "Mechanical Behavior of Inplane-Loaded Unsymmetrically Laminated Plates," 46th AIAA/ASME/ASCE/AHS/ASC Structures, Structural Dynamics and Materials Conference, Austin, TX, AIAA Paper 2005-2099, 2005.

[7] Faggiani, A., and Falzon, B., "Optimization Strategy for Minimizing Damage in Postbuckling Stiffened Panels," *AIAA Journal*, Vol. 45, No. 10, 2007, pp. 2520–2528. doi:10.2514/1.26910

[8] Shen, H. S., "Boundary Layer Theory for the Buckling and Postbuckling of an Anisotropic Laminated Cylindrical Shell. Part 1: Prediction Under Axial Compression," *Composite Structures*, Vol. 82, No. 3, 2008, pp. 346–361. doi:10.1016/j.compstruct.2007.01.024

[9] Rai, D. C., "Inelastic Cyclic Buckling of Aluminum Shear Panels," *Journal of Engineering Mechanics*, Vol. 128, No. 11, 2002, pp. 1233–1237. doi:10.1061/(ASCE)0733-9399(2002)128:11(1233)

[10] Jain, S., Rai, D. C., and Sahoo, D. R., "Postyield Cyclic Buckling Criteria for Aluminum Shear Panels," *Journal of Applied Mechanics*, Vol. 75, No. 2, 2008, Paper 021015. doi:10.1115/1.2793135

[11] Alinia, M. M., and Dastfan, M., "Cyclic Behaviour, Deformability and Rigidity of Stiffened Steel Shear Panels," *Journal of Constructional Steel Research*, Vol. 63, No. 4, 2007, pp. 554–563. doi:10.1016/j.jcsr.2006.06.005

[12] Yoon, S., Honga, S. G., Lee, S. B., and Kim, B. S., "Low Cycle Fatigue Testing of 429EM Stainless Steel Pipe," *International Journal of Fatigue*, Vol. 25, No. 9–11, 2003, pp. 1301–1307. doi:10.1016/j.ijfatigue.2003.08.015

[13] Weller, T., and Singer, J., "Durability of Stiffened Composite Panels Under Repeated Buckling," *International Journal of Solids and Structures*, Vol. 26, No. 9, 1990, pp. 1037–1069. doi:10.1016/0020-7683(90)90016-O

[14] Abramovich, H., Singer, J., and Weller, T., "Repeated Buckling and Its Influence on the Geometrical Imperfections of Stiffened Cylindrical Shells Under Combined Loading," *International Journal of Non-Linear Mechanics*, Vol. 37, Nos. 4–5, 2002, pp. 577–588. doi:10.1016/S0020-7462(01)00085-3

[15] Bisagni, C., Cordisco, P., Abramovich, H., and Weller, T., "Cyclic Buckling Tests of CFRP Curved Panels," International Council on the Aeronautical Sciences 2006 (ICAS), Hamburg, Germany, Paper 10.4.5, 2006.

[16] Degenhardt, R., and Tessmer, J., "Improved Design Scenario for Composite Airframe Structures," 48th AIAA Conference on Structures, Structural Dynamics and Materials, Waikiki, HI, AIAA Paper 2007-2180, 2007.

[17] Arbocz, J., and Starnes, J. H., Jr., "Future Directions and Challenges in Shell Stability Analysis," *Thin-Walled Structures*, Vol. 40, No. 9, 2002, pp. 729–754. doi:10.1016/S0263-8231(02)00024-1

[18] Degenhardt, R., Rolfes, R., Zimmermann, R., and Rohwer, K., "COCOMAT—Improved Material Exploitation at Safe Design of Composite Airframe Structures by Accurate Simulation of Collapse," *Composite Structures*, Vol. 73, No. 2, 2006, pp. 175–178. doi:10.1016/j.compstruct.2005.11.042

[19] Abramovich, H., Weller, T., and Bisagni, C., "Buckling Behavior of Composite Laminated Stiffened Panels Under Combined Shear-Axial Compression," *Journal of Aircraft*, Vol. 45, No. 2, 2008, pp. 402–413. doi:10.2514/1.27635

[20] Cordisco, P., and Bisagni, C., "Design, Test and Validation of a Composite Box Under Combined Loading up to Collapse," *International Journal of Structural Stability and Dynamics* (accepted for publication).

[21] Bisagni, C., and Cordisco, P., "Post-Buckling and Collapse Experiments of Stiffened Composite Cylindrical Shells Subjected to Axial Loading and Torque," *Composite Structures*, Vol. 73, No. 2, 2006, pp. 138–149. doi:10.1016/j.compstruct.2005.11.055

[22] Zhang, X., and Han, Q., "Buckling and Postbuckling Behaviors of Imperfect Cylindrical Shells Subjected to Torsion," *Thin-Walled Structures*, Vol. 45, No. 12, 2007, pp. 1035–1043. doi:10.1016/j.tws.2007.07.003

[23] Arbocz, J., and Babcock, C. D., Jr., "Experimental Investigation of the Effect of General Imperfections on the Buckling of Cylindrical Shells," NASA CR-1163, 1968.

[24] Meyer-Piening, H. R., Farshad, M., Geier, B., and Zimmermann, R., "Buckling Load of CFRP Composite Cylinders Under Combined Axial and Torsion Loading—Experiments and Computations," *Composite Structures*, Vol. 53, No. 4, 2001, pp. 427–435. doi:10.1016/S0263-8223(01)00053-8

[25] Stiftinger, M. A., Skrna-Jakl, I. C., and Rammerstorfer, F. G., "Buckling and Post-Buckling Investigations of Imperfect Curved Stringer-Stiffened Composite Shells. Part B: Computational Investigations," *Thin-Walled Structures*, Vol. 23, No. 1–4, 1995, pp. 339–350. doi:10.1016/0263-8231(95)00021-5

K. Shivakumar
Associate Editor